FINDING BICHROMATIC-BIDIRECTIONAL WAVES WITH ADVS

Mario G. de Souza e Silva[1], Nils B. Kerpen[2], Paulo Cesar C. Rosman[1], Torsten Schlurmann[2], Claudio F. Neves[1]

The aim of this study is to investigate Bichromatic-Bidirectional waves to characterize the subtractive wave-wave nonlinear interactions, using adaptive techniques rather than traditional spectral techniques. A physical model test in a 3D-wave basin was conducted and measurements were made with two arrays of ultrasonic sensors of free surface and one array of ADVs. The Hilbert-Huang transform, aided by the Multivariate Empirical Mode Decomposition, was applied to the orbital velocity data and the main characteristics of the infragravity wave (velocity amplitude, period and direction) were extracted with a good precision.

Keywords: infragravity wave; orbital velocity; Hilbert-Huang transform

INTRODUCTION

Bichromatic-Bidirectional waves (referred as Bi-Bi waves from now on) may be a feature found in Nature more often than expected. Wherever double peaked spectra are found, there is a potential condition for the existence of sea states originated in different regions and coexisting at a given time and location. Sharma and Dean (1981) have presented the theoretical basis on second order in wave steepness for computing wave-wave interactions. The authors associated the difference/addition of frequencies to the difference/addition of wave number vectors, took a pair of frequencies within the spectrum and obtained the subtractive/additive interference waves, besides the self-interacting (second order) of each primary wave. After developing the equations for the velocity potential, they could finally compute the forces on cylinders for the primary waves, including the second order interferences (both high and low frequency).

In coastal regions, the subtractive interference, usually related to infragravity waves, may be significant over the hydrodynamics and morphodynamics of sandy beaches, tidal inlets, coral reefs and harbors (Bertin et al. 2018). These long period oscillations can drive rip currents (Dalrymple et al. 2011); propagate into aquifers on sandy coasts and cause underground water fluxes through barrier islands, between sea and lagoons (Longuet-Higgins 1983; Li and Barry 2000; Geng and Boufadel 2015); can intensify wave run-up and overtopping over dunes, structures and fringing coral reefs (Cheriton, Storlazzi, and Rosenberger 2016); and can eventually dominate the net sediment transport in the surf zone (Aagaard and Greenwood 2008). Janssen (2003) reported that the slow modulation of the infragravity waves can cause resonance inside harbors, affecting the moored ship behavior and the design wave height for port structures. According to the author, the forcing of infragravity waves may even "be normative to their design". Infragravity waves have been associated with microseisms (Longuet-Higgins 1950); can cause vibrations in coastal cliffs, leading to their instability and erosion (Young et al. 2011); and are related to seismic waves in the solid Earth, a phenomenon known as "the hum" (Ardhuin, Gualtieri, and Stutzmann 2015).

Although the existence of infragravity waves has been known since the first observations of long period motions made by Munk (1949) and Tucker (1950), the directional properties of infragravity waves are seldom addressed. Nose, Babanin, and Ewans (2016) attribute this lack of studies and measurements to the "complexity of their generation mechanisms and the inherent difficulties related to detection of very small signal gradients over a period of up to a few minutes". To study the directionality of infragravity waves produced by wind waves, they applied the Fourier Transform (FFT) and the Maximum Entropy Method (MEM) to their wind-wave measurements (pressure and horizontal velocities). However, although the Fourier analysis has been the standard wave data analysis tool in Coastal Engineering, it is well known that FFT is essentially suitable for stationary and linear phenomena.

The focus of the present work is to capture the subtractive interference wave kinematic characteristics (velocity amplitude, period and direction) generated by Bi-Bi waves in a 3D wave basin,

[1] Ocean Engineering Program, Federal University of Rio de Janeiro, Av. Horácio de Macedo 2030, Bloco C, Sala 203, Rio de Janeiro, RJ, 21941-972, Brazil

[2] Ludwig-Franzius-Institute, Leibniz University Hannover, Nienburger Straße 4, Hannover, Lower Saxony, 30167, Germany

using ADV measurements and subsequent application of the Hilbert-Huang Transform (HHT). Because of its three-dimensional nature, velocities give a more complete description of the sea state than wave heights. On the other hand, ADVs are more sensitive than surface piercing wave gauges. Although ADV outputs are often filled up with noise and spikes, caused by lack of reflecting particles in the water or turbulence in the flow, a robust post-processing technique was developed which will be described later. The HHT was chosen for its capacity of analyzing non-stationary and non-linear phenomena (Huang et al. 1998).

EXPERIMENTAL STUDIES

Bi-Bi waves were generated in the 30 m × 15 m wave basin of the Ludwig-Franzius-Institute for Hydraulic, Estuarine and Coastal Engineering of the Leibniz University Hannover, where 72 independent paddles are positioned along the longest side and a 5 m wide passive absorption system is placed on the other three sides of the basin, as shown in Figure 1. The experiments aimed to identify the subtractive second order orbital velocities using one array of 5 ADVs. Two arrays with 5 and 6 ultrasonic sensors of free surface elevation were also used for comparison between different types of measurements.

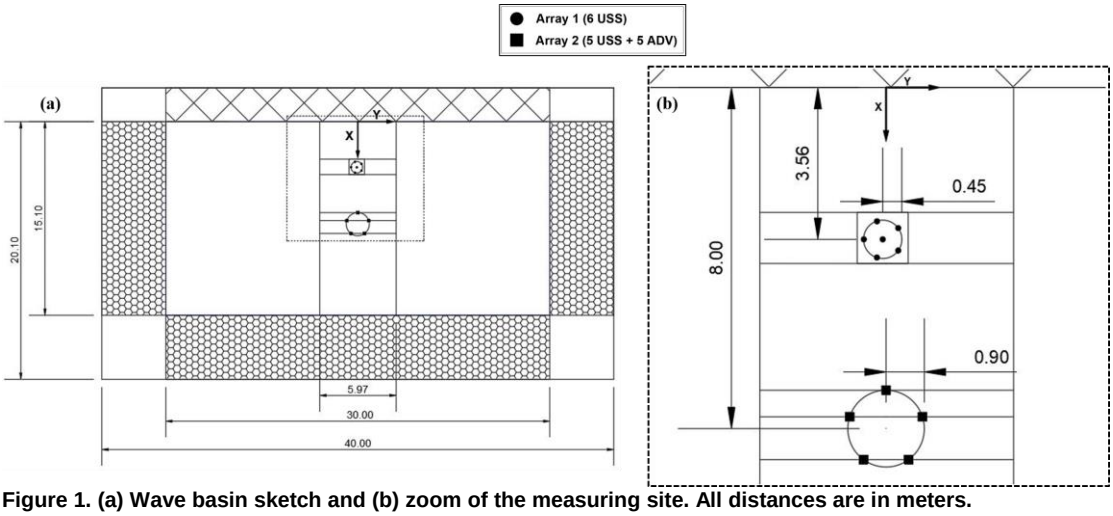

Figure 1. (a) Wave basin sketch and (b) zoom of the measuring site. All distances are in meters.

Figure 2. Example of a Bi-Bi wave simulation with focus on the ADV array.

A total of 271 tests, each with 2 minutes duration, were simulated, including full bimodal seas and repetition tests for statistical significance. The following conditions were tested: water depth of 0.60 m and 0.75 m; wave heights ranging from 0.05 m to 0.16 m; periods ranging from 1.1 s to 3.0 s; angle differences between primary waves of 0°, 10° and 30°. Figure 2 shows an example of Bi-Bi waves simulation, with a focus on array 2. The ADVs were positioned mainly at a depth of 0.35 m, but a few

experiments had the instruments at 0.50 m below the free surface. Table 1 summarizes the main characteristics of each group of tests simulated and Table 2 the Bi-Bi waves conditions for one specific subgroup of tests.

Note that experiments T4-A, T6-B and T4-C have the same angle difference between them, but the angles of the primary waves are different between T4-A/T6-B and T4-C. As Sand (1982) pointed out, the wave number of the infragravity wave ($\bar{k}$) is given by the subtraction of the wave number vectors of the primary waves. Therefore, $\bar{k}$ of tests T4-A/T6-B and T4-C will have the same magnitude and almost the same direction (28.16° and 23.16°, respectively).

Table 1. Main characteristics of each test group (h = water depth; d = ADV depth; H_a and H_b = wave heights; T = wave period; and D = wave direction).

Test	h (m)	d (m)	H_a (m)	H_b (m)	T (s)	D (°)
T1	0.60	0.35	0.13	0.13	Combination of 3 different periods (1.1<T< 3.0)	Combination of 3 different angle differences (0°, 10°, 30°)
T2	0.60	0.35	0.10	0.16		
T3	0.75	0.35	0,13	0.13		
T4	0.75	0.35	0.10	0.16		
Extra Tests						
T5	0.60	0.35	0.05	0.11		
T6	0.75	0.50	0.10	0.16		
T7	0.60	0.35	0.10	0.16	Statistical Repetition	
T8	Bimodal Spectra					

Table 2. Sample of experimental tests made in the 3D wave basin.

Teste	H_a (m)	H_b (m)	T_a (s)	T_b (s)	D_a (°)	D_b (°)	h (m)	d (m)
T4-A	0.10	0.16	1.3	1.7	10	0	0.75	0.35
T6-B	0.10	0.16	1.3	1.7	10	0	0.75	0.50
T4-C	0.10	0.16	1.3	1.7	5	-5	0.75	0.35
T4-D	0.10	0.16	1.3	1.7	30	0	0.75	0.35

METHODOLOGY

Usually ADV data contains a lot of noise and spikes which mask the underlying useful data. Before applying the Hilbert-Huang Transform to the velocity measurements, three post-processing analysis were used to clean the raw ADV output:

1. Despiking: spikes are anomalies in the data that can be caused by aleatory movement of suspended material in the measurement site (Voulgaris and Trowbridge 1998), phase wrapping (Rusello 2009), air bubbles (Liu, Zhu, and Rajaratnam 2002), bottom interference (Lane et al. 1998) or lack of suspended material in the water column (Lykke Andersen, Eldrup, and Frigaard 2017). In this work, spikes were eliminated according to the method proposed by Goring and Nikora (2002);
2. Data filtering: the high sensitivity of the ADV probes are able to capture even small magnitude hydrodynamic phenomena, as turbulence. As the main objective of this paper is to analyze low frequency motions, the ADV output was filtered with a low pass filter (Thompson 1983), which kept third order interaction components;
3. Tilt correction: in practice, it is very hard to align the probes exactly in the planned position. Different than the field probes, laboratory ADVs do not contain a compass for tilt correction. If even small misalignments exist, each velocity component will be affected by the other, contaminating the true data. Therefore, the square cross-correlation matrix procedure proposed by Neves et al. (2012) was applied to correct the ADV tilting.

Figure 3 shows the time series of one component and the 3D hodograph of the measured velocities after the three-step procedure and a comparison with the modeled velocities given by the Sharma and Dean (1981) equations.

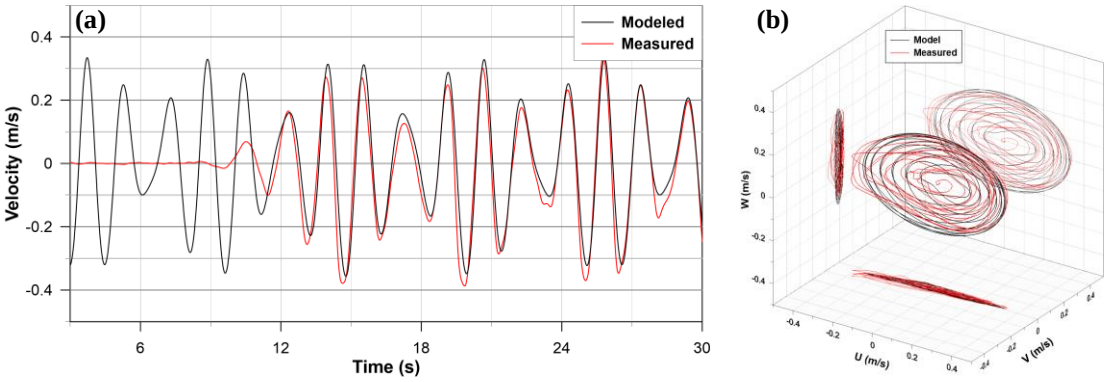

Figure 3. Comparison between modeled and post-processed measured velocity for case T4-A. (a) Horizontal U velocity time series and (b) three-dimensional orbital velocity.

The post-processed orbital velocities were then subjected to the Hilbert-Huang Transform which is a tool designed specifically to deal with non-stationary and non-linear data. The HHT procedure is composed by two steps: (i) time series decomposition through the Empirical Mode Decomposition (EMD); and (ii) Hilbert transform. Instead of decomposing a time series into components with fixed amplitude and frequency, as the FFT, the EMD separates the measurements into Intrinsic Mode Functions (IMFs), which may have variable amplitude and frequency. To each IMF the Hilbert transform is then applied, showing how frequency and amplitude of the phenomena vary in time.

The EMD, however, can only analyze scalar quantities or one-dimensional vector series. As the velocity is a three-dimensional variable, where each component is dependent on the others, the Noise Assisted Multivariate Empirical Mode Decomposition – NA-MEMD (Rehman et al. 2013), was used to assist the HHT. The MEMD can work with multivariate/multidimensional time series and produces mode aligned IMFs, which is desirable for the velocity analysis. White Gaussian distributed noise is added to mathematical dimensions to assist the decomposition procedure.

The capacity of the MEMD to analyze multidimensional time series gave the authors the idea to analyze all 5 ADVs together, as an array, instead of sifting each ADV data separately. As all instruments are measuring the same phenomena of interest, the subtractive wave-wave interaction, it is expected that the mode alignment capability of the MEMD produces one IMF that corresponds to this low frequency oscillation for each velocity component of each ADV data. Therefore, it should be possible to extract the 'infragravity wave' from the Bi-Bi waves velocity records.

RESULTS

In this section, results from the tests shown in Table 2 are shown. A more detailed analysis of all the different tests conditions simulated will be presented in a future paper.

The FFT analysis of the second array of USSs is shown in Figure 4 for case T4-A, where T_a = 1.3 s, T_b = 1.7 s and T^- = 5.525 s. Note that primary waves 'a' and 'b' are clearly identified in the directional energy spectra. However, as wave 'a' has an angle of 10° angle relative to the normal to the wave maker, a large directional spreading is present due to reflection inside the basin. The subtractive wave-wave interaction is also present, with also a wide directional spreading.

Figure 5 shows the HHT result of the array of ADVs for the same test. Only the Hilbert transform of the IMFs that corresponds to the primary waves (IMFs 6 and 7) and the subtractive wave-wave interaction (IMF 9) are plotted. White dashed lines represent the theoretical expected frequencies for this test. It is seen that IMFs 6 and 7 oscillate around the expected frequency. The strong oscillation is due to mode mixing, a common problem faced by the HHT when two different phenomena with close frequencies inhabit the measurement. However, as the subtractive interference wave has a quite distinctive frequency (f^- = 0.18 Hz), its IMF does not suffer from mode mixing and an almost straight line is plotted on top of the expected result.

The extracted low frequency orbital velocities for all tests indicated in Table 2 are presented in Figure 6. The theoretical hodographs calculated by Sharma and Dean (1981) equations are also plotted for comparison. Only 5 wave cycles (≈28 s) are illustrated. It is visually clear the similarity between theory and the results from the HHT method. A more precise deviation measure between the extracted

and the theoretical velocities can be given by the 3D Root Mean Square Error ($RMSE_{3D}$) defined by equation (1).

$$\mathrm{RMSE}_{3\mathrm{D}} = \sqrt{\mathrm{RMSE}_{\mathrm{U}}^2 + \mathrm{RMSE}_{\mathrm{V}}^2 + \mathrm{RMSE}_{\mathrm{W}}^2} \qquad (1)$$

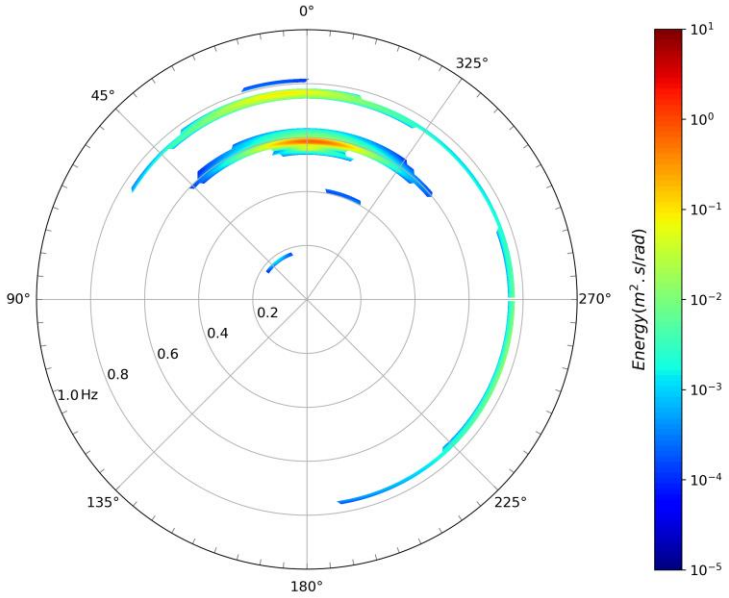

Figure 4. Wave energy spectrum of case T4-A calculated from the second array of ultrasonic sensors.

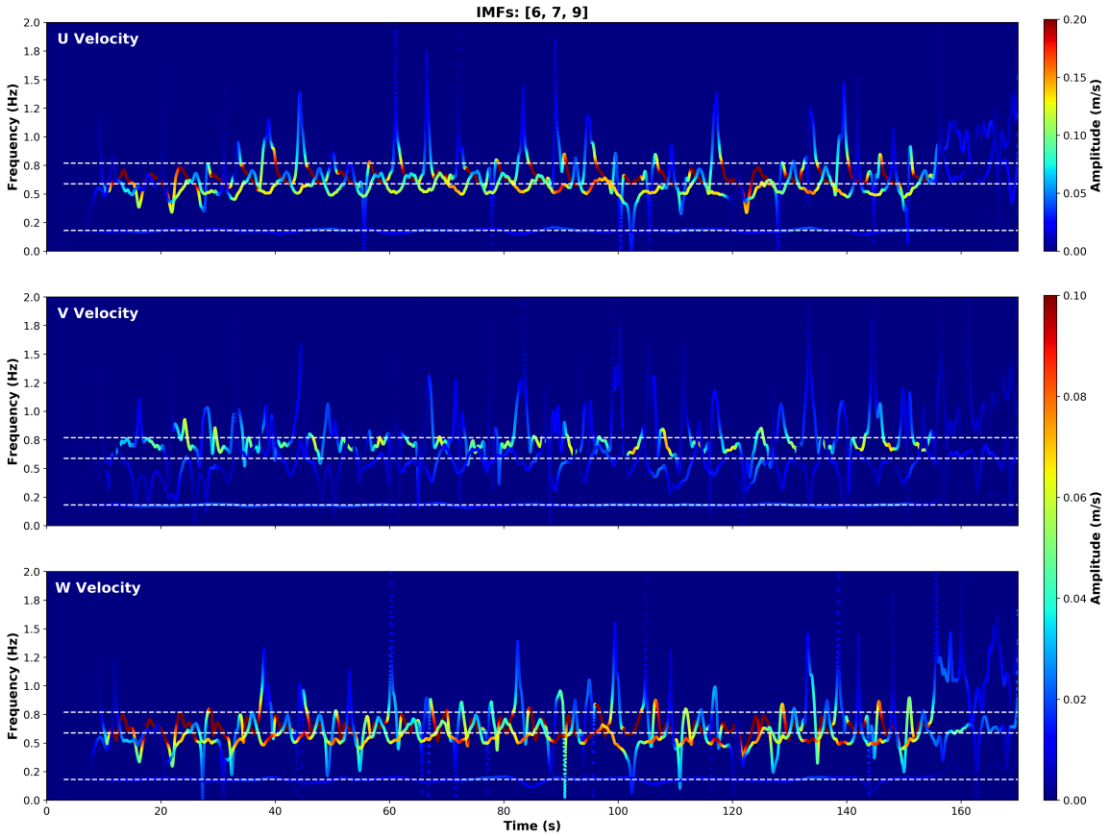

Figure 5. Hilbert-Huang Transform of the measured velocities U, V and W, respectively, for case T4-A. Only the IMFs from the primary (6 and 7) and subtractive interference (9) waves are shown.

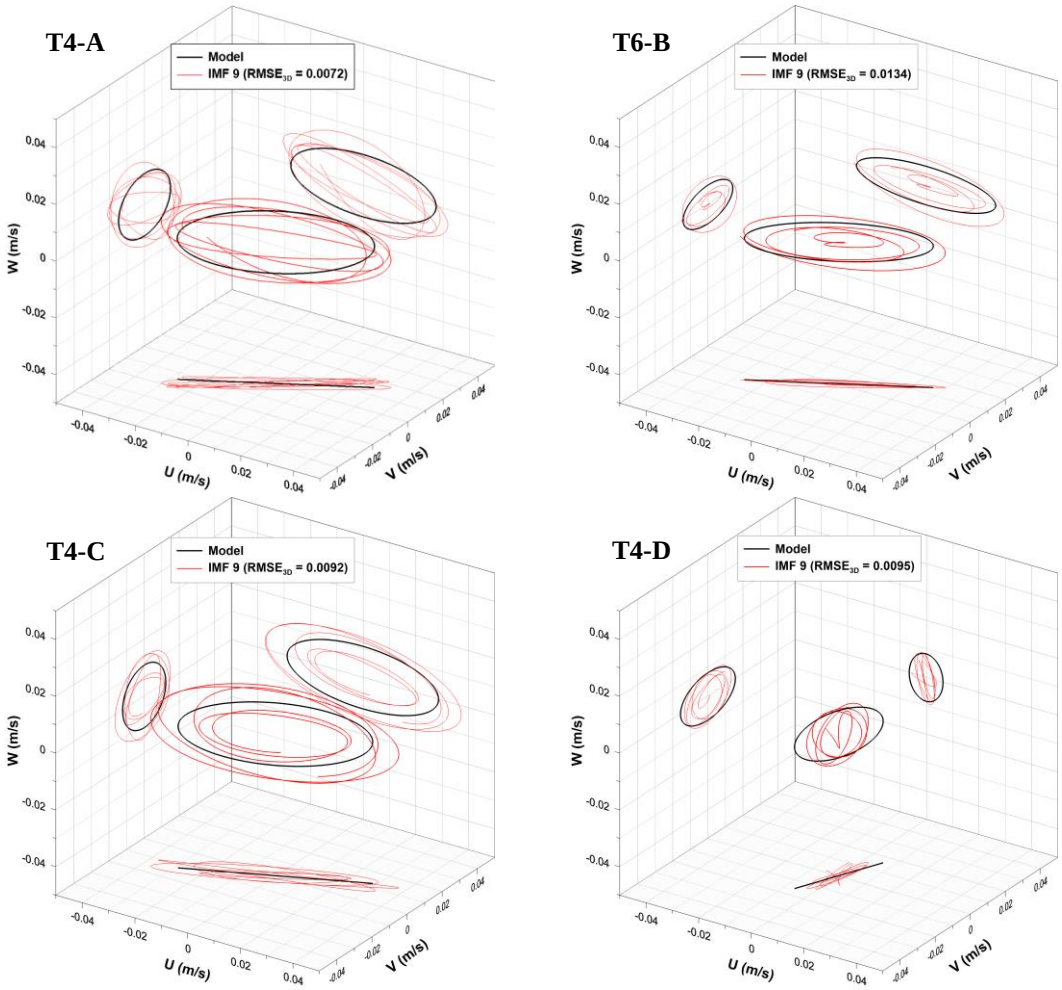

Figure 6. Comparison between modeled (Sharma and Dean, 1981) and extracted (HHT) subtractive wave-wave interaction generated by Bi-Bi waves of cases T4-A, T6-B, T4-C and T4-D.

CONCLUSION

Analysis of the orbital velocities proved to be more accurate than the free surface elevation regarding the determination of non-linear interaction effects. The HHT method captured the amplitude, direction and frequency of the subtractive wave-wave interaction with good agreement with theory. The NA-MEMD algorithm has shown a remarkable capability for isolating the low frequency wave from the primary Bi-Bi waves. However, mode mixing between the primary waves are still present and demand further effort to improve the HHT capability.

ACKNOWLEDGEMENTS

This study was financed in part by the Coordenação de Aperfeiçoamento de Pessoal de Nível Superior - Brasil (CAPES Foundation) - Finance Code 001. The authors acknowledge and are thankful for the technical, financial, material, and personnel support provided by the Ludwig-Franzius-Institute of the Leibniz University Hannover to do the experiments, and the support of the Ocean Engineering Program / COPPE of the Federal University of Rio de Janeiro.

REFERENCES

Aagaard, T., and B. Greenwood. 2008. Infragravity Wave Contribution to Surf Zone Sediment Transport — The Role of Advection, *Marine Geology*, 251 (1–2): 1–14.

Ardhuin, F., L. Gualtieri, and E. Stutzmann. 2015. How Ocean Waves Rock the Earth: Two Mechanisms Explain Microseisms with Periods 3 to 300 S, *Geophysical Research Letters*, 42 (3):

765–72.
Bertin, X., A. Bakker, A. Dongeren, G. Coco, G. André, F. Ardhuin, P. Bonneton, et al. 2018. Infragravity Waves: From Driving Mechanisms to Impacts, *Earth-Science Reviews*, January.
Cheriton, O.M., C.D. Storlazzi, and K.J. Rosenberger. 2016. Observations of Wave Transformation over a Fringing Coral Reef and the Importance of Low-Frequency Waves and Offshore Water Levels to Runup, Overwash, and Coastal Flooding, *Journal of Geophysical Research: Oceans*, 121 (5): 3121–40.
Dalrymple, R.A., J.H. MacMahan, A.J.H.M. Reniers, and V. Nelko. 2011. Rip Currents, *Annu. Rev. Fluid Mech.*, 43 (1): 551–81.
Geng, X., and M.C. Boufadel. 2015. Numerical Study of Solute Transport in Shallow Beach Aquifers Subjected to Waves and Tides, *Journal of Geophysical Research: Oceans*, 120 (2): 1409–28.
Goring, D.G, and V.I. Nikora. 2002. Despiking Acoustic Doppler Velocimeter Data, *Journal of Hydraulic Engineering*, 128 (1): 117–26.
Huang, N.E, Z. Shen, S.R. Long, M.C. Wu, H.H. Shih, Q. Zheng, N.-C. Yen, C.C Tung, and H.H. Liu. 1998. The Empirical Mode Decomposition and the Hilbert Spectrum for Nonlinear and Non-Stationary Time Series Analysis, *Proceedings of the Royal Society A: Mathematical, Physical and Engineering Sciences*, 454 (1971): 903–95.
Janssen, T.T. 2003. Long Waves Induced by Short-Wave Groups over a Sloping Bottom, *Journal of Geophysical Research*, 108 (C8): 3252.
Lane, S.N., P.M. Biron, K.F. Bradbrook, J.B. Butler, J.H. Chandler, M.D. Crowell, S.J. McLelland, K.S. Richards, and A.G. Roy. 1998. Three-dimensional Measurement of River Channel Flow Processes Using Acoustic Doppler Velocimetry, *Earth Surface Processes and Landforms*, 23 (13): 1247–67.
Li, L., and D.A. Barry. 2000. Wave-Induced Beach Groundwater Flow, *Advances in Water Resources*, 23 (4): 325–37.
Liu, M., D.Z. Zhu, and N. Rajaratnam. 2002. Evaluation of ADV Measurements in Bubbly Two-Phase Flows, In: *Hydraulic Measurements and Experimental Methods Specialty Conference (HMEM) 2002*, ASCE.
Longuet-Higgins, M.S. 1950. A Theory of the Origin of Microseisms, *Philosophical Transactions of the Royal Society A: Mathematical, Physical and Engineering Sciences*, 243 (857): 1–35.
Longuet-Higgins, M.S. 1983. Wave Set-Up, Percolation and Undertow in the Surf Zone, *Proceedings of the Royal Society A: Mathematical, Physical and Engineering Sciences*, 390 (1799): 283–91.
Lykke Andersen, T., M.R. Eldrup, and P. Frigaard. 2017. Estimation of Incident and Reflected Components in Highly Nonlinear Regular Waves, *Coastal Engineering* 119 (January): 51–64.
Munk, W.H. 1949. Surf Beats, *American Geophysical Union*, 30 (6): 849–54.
Neves, C.F., L.M. Endres, J. Fortes, and D. Spinola. 2012. The Use of Adv in Wave Flumes: Getting More Information about Waves, *Coastal Engineering Proceedings* 1 (33): 1–15.
Nose, T., A. Babanin, and K. Ewans. 2016. Directional Analysis and Potential for Spectral Modelling of Infragravity Waves, In: *Volume 7: Ocean Engineering*, V007T06A091. ASME.
Rusello, P.J. 2009. A Practical Primer for Pulse Coherent Instruments, Technical Note TN-027,
Sand, S.E. 1982. Long Waves in Directional Seas, *Coastal Engineering* 6 (3): 195–208.
Sharma, J.N., and R.G. Dean. 1981. Second-Order Directional Seas and Associated Wave Forces. *Society of Petroleum Engineers Journal*, 21 (01): 129–40.
Thompson, R.O.R.Y. 1983. Low-Pass Filters to Suppress Inertial and Tidal Frequencies, *Journal of Physical Oceanography*, 13 (6): 1077–83.
Tucker, M.J. 1950. Surf Beats: Sea Waves of 1 to 5 Min. Period, *Proceedings of the Royal Society A: Mathematical, Physical and Engineering Sciences*, 202 (1071): 565–73.
Rehman, N.U., C. Park, N.E. Huang, and D.P. Mandic. 2013. EMD via MEMD: Multivariate Noise-Aided Computation of Standard EMD, *Advances in Adaptive Data Analysis*, 05 (02): 1350007.
Voulgaris, G., and J.H. Trowbridge. 1998. Evaluation of the Acoustic Doppler Velocimeter (ADV) for Turbulence Measurements, *Journal of Atmospheric and Oceanic Technology*, 15 (1): 272–89.
Young, A.P., P.N. Adams, W.C. O'Reilly, R.E. Flick, and R.T. Guza. 2011. Coastal Cliff Ground Motions from Local Ocean Swell and Infragravity Waves in Southern California, *Journal of Geophysical Research*, 116 (C9): C09007.